Flow diagram of the metal–insulator transition in two dimensions

S. ANISSIMOVA[1], S. V. KRAVCHENKO[1]*, A. PUNNOOSE[2], A. M. FINKEL'STEIN[3] AND T. M. KLAPWIJK[4]

[1]Physics Department, Northeastern University, Boston, Massachusetts 02115, USA
[2]Physics Department, City College of the City University of New York, New York, New York 10031, USA
[3]Department of Condensed Matter Physics, Weizmann Institute of Science, Rehovot 76100, Israel
[4]Kavli Institute of Nanoscience, Faculty of Applied Sciences, Delft University of Technology, 2628 CJ Delft, The Netherlands
*e-mail: s.kravchenko@neu.edu

The discovery of the metal–insulator transition (MIT) in two-dimensional electron systems[1] challenged the veracity of one of the most influential conjectures[2] in the physics of disordered electrons, which states that 'in two dimensions, there is no true metallic behaviour'; no matter how weak the disorder, electrons would be trapped and unable to conduct a current. However, that theory did not account for interactions between the electrons. Here, we investigate the interplay between the electron–electron interactions and disorder near the MIT using simultaneous measurements of electrical resistivity and magnetoconductance. We show that both the resistance and interaction amplitude exhibit a fan-like spread as the MIT is crossed. From these data, we construct a resistance–interaction flow diagram of the MIT that clearly reveals a quantum critical point, as predicted by the two-parameter scaling theory[3]. The metallic side of this diagram is accurately described by the renormalization-group theory[4] without any fitting parameters. In particular, the metallic temperature dependence of the resistance sets in when the interaction amplitude reaches $\gamma_2 \approx 0.45$—a value in remarkable agreement with the one predicted by theory[4].

The low amount of disorder in high-mobility silicon metal-oxide–semiconductor field-effect transistors (Si MOSFETs) allows measurements to be made in the regime of very low electron densities where correlation effects due to electron–electron interactions become especially important. (Ratios $r_s \equiv E_C/E_F > 10$ between Coulomb and Fermi energies are easily reached with Fermi energies of the order 0.7 meV.) This material system has the further advantage that its electron spectrum has two almost degenerate valleys, which further enhances the correlation effects. Indeed, the low-temperature drop of the resistance on the metallic side of the transition (Fig. 1a) in Si MOSFETs is the most pronounced among all two-dimensional (2D) electron systems[5,6].

At low temperatures $k_B T < \hbar/\tau < E_F$, electrons propagate diffusively. Here, k_B is Boltzmann's constant, T is temperature and τ is the electron mean free time. This region, referred to as the diffusive regime, extends up to a few kelvin near the metal–insulator transition (MIT). As a result, the low-temperature physics of the disordered electron liquid, combined with the large r_s values near the MIT, is determined by the properties of interacting, diffusing electrons[7–9].

With this in mind, and with the view of studying the role of disorder and effective strengths of the electron interactions in the vicinity of the MIT, we have carried out simultaneous measurements of the resistivity, ρ, and

in-plane magnetoconductance, $\sigma(B)$. As the origin of the magnetoconductance lies in the interaction corrections to the conductance involving different spin projections (Hartree-like), the corresponding interaction strength can be determined from the slope of $\sigma(B)$. When a magnetic field, B, is applied parallel to the 2D plane in the diffusive regime[10,11], the magnetoconductance $\Delta\sigma(B,T) \equiv \sigma(B,T) - \sigma(0,T)$ is proportional to b^2 in the weak-field limit $b \equiv g\mu_B B/k_B T \ll 1$, where μ_B is the Bohr magneton. On the other hand, at higher temperatures $\hbar/\tau < k_B T < E_F$, referred to as the ballistic regime, $\Delta\sigma(B,T)$ is expected to be proportional to Tb^2 (ref. 12). Because the magnetoconductivities in these two regions are so different, measuring $\Delta\sigma(B,T)$ provides a reliable way to identify the diffusive region.

The samples we used had peak electron mobilities of about 3×10^4 cm^2 V^{-1} s^{-1} at 0.2 K. The resistivity, ρ, was measured by a standard low-frequency lock-in technique. The magnetoresistance traces, $\rho(B)$, for a representative density in the diffusive region $n_s = 9.14 \times 10^{10}$ cm^{-2}, are plotted in Fig. 2a for different temperatures; $\rho(T)$ at $B = 0$ for this density is the third curve from the bottom in Fig. 1a. The corresponding magnetoconductivities, $\Delta\sigma = 1/\rho(B) - 1/\rho(0)$, are plotted as function of b^2 in Fig. 2b. When plotted this way, it can be seen that the $\sigma(b^2)$ curves are linear. It can also be seen that the slopes decrease slowly with temperature. This is important, because had the electrons been in the ballistic regime, the slopes would have instead increased with temperature by an order of magnitude in the temperature interval used owing to the expected Tb^2 dependence. By applying the same procedure to different electron densities, we find that the diffusive region extends to approximately 25% in electron densities above the critical density of the MIT. (The critical density $n_c \approx 8 \times 10^{10}$ cm^{-2} in this sample.)

The explicit form of the slope of $\Delta\sigma(b^2)$ for the single-valley case was derived in refs 10,11. It is straightforward to accommodate the valley degrees of freedom. For the case of n_v degenerate valleys ($n_v = 2$ for silicon), we obtain for $\Delta\sigma(b^2)$, in the limit $b \ll 1$, the expression

$$\Delta\sigma(b^2) = -0.091 \frac{e^2}{\pi h} n_v^2 \gamma_2 (\gamma_2 + 1) b^2. \qquad (1)$$

(We note that the constant 0.091 in equation (1) provides a more accurate coefficient compared with the value 0.084 given in ref. 10.) Here, γ_2 is the effective electron–electron interaction amplitude in the spin-density channel. (In standard Fermi-liquid notation, γ_2 is related to the parameter F_0^a as $\gamma_2 = -F_0^a/(1 + F_0^a)$.) As was observed
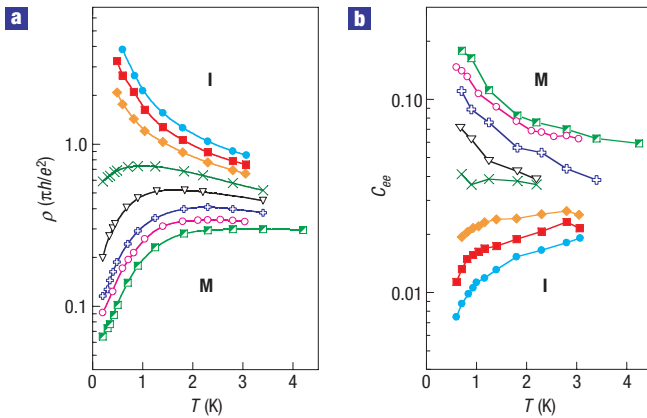
Figure 1 Temperature dependencies of the resistivity and of the strength of spin-related interactions for electron densities across the MIT. **a**, $\rho(T)$ traces at $B = 0$. **b**, $C_{ee}(T)$, extracted from the slope of the magnetoconductance (see text). Both $\rho(T)$ and $C_{ee}(T)$ exhibit a fan-like structure across the MIT. The densities (in units of 10^{10} cm^{-2}) are: 7.24, 7.53, 7.83, 8.26, 8.70, 9.14, 9.58 and 9.87. In **a**, the densities increase from top to bottom, whereas in **b**, they increase from bottom to top, that is, the interaction increases in the metallic phase and decreases in the insulating phase as the temperature is lowered. **M** and **I** regions indicate metallic and insulating phases, respectively.
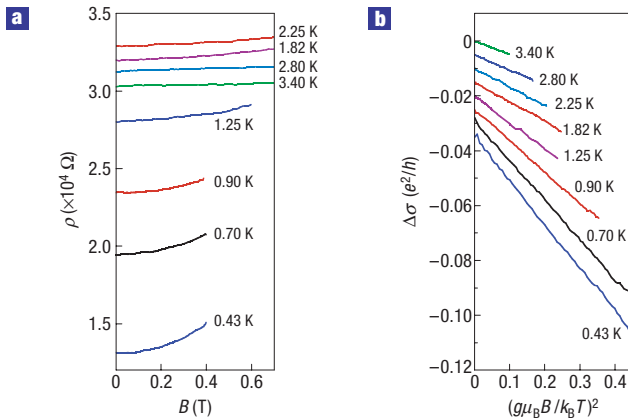

Figure 3 The disorder–interaction (ρ–C_{ee}) flow diagram of the 2D electron liquid in Si MOSFETs. The red circle at $\rho \approx 0.8$ and $C_{ee} \approx 0.035$ indicates the location of the QCP from which the three separatrices (black lines) emanate. The arrows indicate the direction of the flow as the temperature is lowered. The electron densities are indicated in units of 10^{10} cm^{-2}.

Figure 2 Magnetoresistivity and magnetoconductivity for electron density $n_s = 9.14 \times 10^{10}$ cm^{-2} measured at different temperatures. **a**, Resistivity plotted against magnetic field applied parallel to the 2D plane. **b**, Magnetoconductivity $\Delta\sigma(B, T) \equiv \sigma(B, T) - \sigma(0, T)$ (in units of the quantum conductance) plotted as a function of $(g\mu_B B/k_B T)^2$. The curves in **b** are vertically shifted for clarity. Note that the curves for different temperatures are linear when plotted versus $(g\mu_B B/k_B T)^2$ and their slopes slowly decrease with temperature.

earlier in ref. 4, the large factor n_v^2 due to the valleys enhances the effect of the e–e interactions. (Here, we have assumed that the valleys are fully degenerate at all temperatures by restricting ourselves to $T > T_v$, where T_v is the temperature scale associated with the valley splitting. This temperature is not precisely known, but our analysis of the low-temperature data suggests $T_v \approx 0.5$ K. Further details of this region will be presented elsewhere.)

Equation (1), as was shown in ref. 11, incorporates renormalization-group corrections to first order in ρ and is therefore strictly valid only deep in the metallic region. For
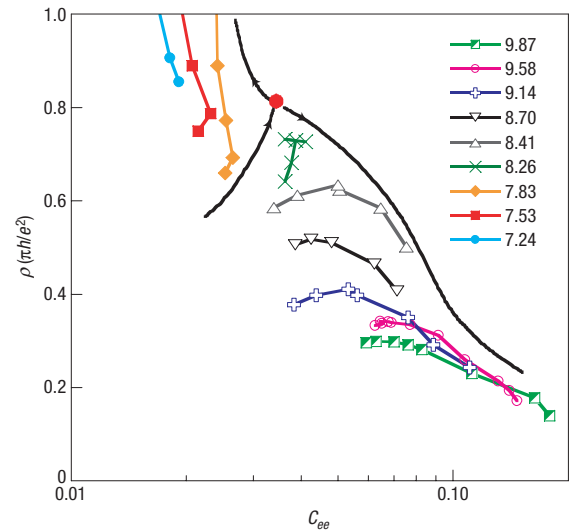
general ρ, the magnetoconductance in the diffusive regime will still retain the b^2 form, $\Delta\sigma = -(e^2/\pi h)C_{ee}(\gamma_2, \rho)n_v^2 b^2$. The coefficient C_{ee} reflects the strength of spin-related interactions at any value of the resistance (as long as $g\mu_B B < k_B T < h/\tau$). This is because the in-plane magnetoconductance is a consequence of the splitting of the spin sub-bands. The fluctuations in spin density lead to finite temperature corrections to the resistivity via the electron–electron interaction amplitude in the spin-density channel, γ_2. Thus, the spin splitting, by reducing these fluctuations, leads to a finite magnetoconductance through γ_2.

The temperature dependences of the parameter C_{ee}, extracted by fitting the $\sigma(b^2)$ traces in Fig. 2b, are shown in Fig. 1b for various densities across the MIT. To the best of our knowledge, this is the first observation of the temperature dependence of the strength of the electron–electron interactions. In Fig. 1a, we plot $\rho(T)$ at zero magnetic field for the same densities. (In the following, ρ is always expressed in units of $\pi h/e^2$ (ref. 3).) Figure 1 reveals that not only ρ but also the interaction strength exhibits a fan-like spread as the MIT is crossed. We see that, whereas the interaction grows in the metallic phase as the temperature is reduced, it is suppressed in the insulating phase. The magnitudes of these changes depend on how far the system is from the MIT, with both ρ and γ_2 becoming practically temperature independent for densities close to the MIT. This behaviour is indicative of the flow around a quantum critical point (QCP), which is fully consistent with the theoretical prediction that the evolution of ρ and the interaction amplitude, γ_2, with temperature are described by a two-parameter system of coupled renormalization-group equations manifesting an unstable fixed point corresponding to the QCP[3]. Note that a phase diagram can be presented in different coordinates obtained as a result of various (rather broad) transformations, preserving the topology of the phase diagram. In our case, the transformation involves using the slope of the magnetoconductance.

To see this in a different way, we combine Fig. 1a and b and construct a two-parameter 'flow' diagram in the disorder–interaction (ρ–C_{ee}) space. The flow diagram is shown
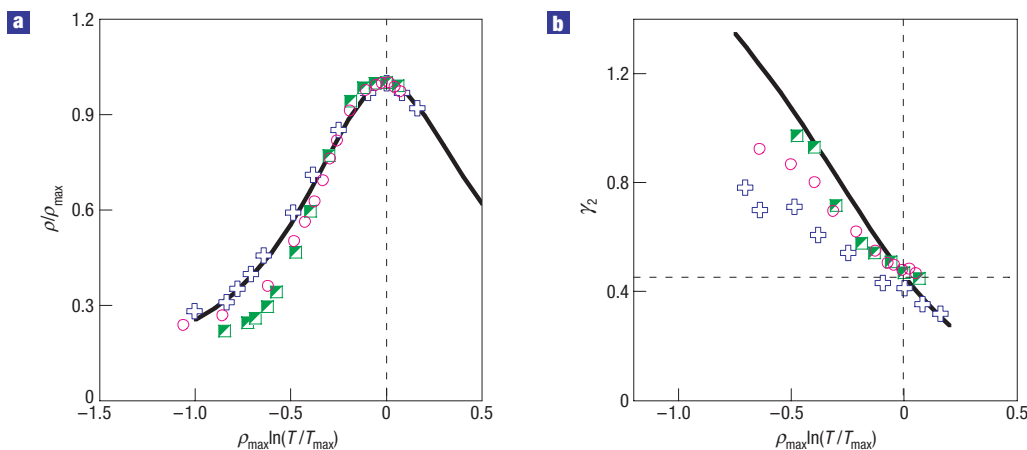
Figure 4 Comparison between theory (lines) and experiment (symbols). a, ρ/ρ_{max} as a function of $\rho_{max}\ln(T/T_{max})$. **b**, γ_2 as a function of $\rho_{max}\ln(T/T_{max})$. The vertical dashed lines correspond to $T = T_{max}$, the temperature at which $\rho(T)$ reaches the maximum. Note that at this temperature, the interaction amplitude $\gamma_2 \approx 0.45$ (indicated by the horizontal dashed line in **b**), in excellent agreement with theory. The symbols are the same as in Figs 1 and 3 and correspond to $n_s = 9.87$, 9.58 and 9.14×10^{10} cm^{-2}.

in Fig. 3. It can be seen that such a flow diagram constructed out of ρ and the parameter C_{ee} (which is sensitive to the amplitude γ_2) clearly indicates the existence of a QCP from which three separatrices, one attractive and two repulsive, can be drawn.

On the metallic side of the flow diagram, a separatrix that forms the envelope of a family of non-monotonic curves can be clearly seen in Fig. 3 flowing towards the region with $\rho \ll 1$. The theoretical details of the evolution of ρ and the γ_2 in this region with $\rho \ll 1$ were discussed in detail in ref. 4 in terms of a renormalization-group theory. We recall the salient features of the theory here. The theory predicts that: (1) the amplitude γ_2 increases monotonically as the temperature is reduced; (2) the resistance, on the other hand, has a characteristic non-monotonic form changing from insulating behaviour ($d\rho/dT < 0$) at high temperatures to metallic behaviour ($d\rho/dT > 0$) at low temperatures, with the maximum value, ρ_{max}, occurring at a crossover temperature $T = T_{max}$; (3) the value of the amplitude γ_2 at $T = T_{max}$ is universal in the limit $\rho_{max} \ll 1$, depending only on n_v; for $n_v = 1$, it is 2.08, whereas for $n_v = 2$, it has the much lower value 0.45; (4) although the values of ρ_{max} and T_{max} are not universal and depend on the system, the behaviours of $\rho(T)/\rho_{max}$ and $\gamma_2(T)$ are universal when plotted as functions of $\rho_{max}\ln(T/T_{max})$.

The results of comparison between experiment and theory are shown in Fig. 4a,b, for the three largest densities in the diffusive regime with $\rho_{max} \lesssim 0.4$ $(\pi h/e^2)$. At these densities, the resistance is small enough, and we can safely extract the interaction amplitudes γ_2 from $\Delta\sigma(b^2)$ using equation (1), that is, $C_{ee} = 0.091\gamma_2(1 + \gamma_2)$. (As the density increases, the maximum in $\rho(T)$ becomes less pronounced, and the non-monotonicity eventually disappears at $n_s \gtrsim 1 \times 10^{11}$ cm^{-2}, as the ballistic region is approached.) The solid lines are the universal theoretical curves for $\rho(T)/\rho_{max}$ and $\gamma_2(T)$ plotted as a function of $\rho_{max}\ln(T/T_{max})$. It can be seen from Fig. 4 that at $T = T_{max}$, the value of the interaction amplitude $\gamma_2 \approx 0.45$, which is in remarkable agreement with theory for $n_v = 2$. The agreement between theory and experiment is especially striking given that the theory has no adjustable parameters. Systematic deviations from the universal curve occur at lower densities as higher-order corrections in ρ become important.

The data for γ_2 allow us to calculate the renormalized Landé g-factor $g^* = 2(1 + \gamma_2)$. For our highest density sample, it grows from $g^* \approx 2.9$ at the highest temperature to $g^* \approx 4$

at the lowest. This is the first time the g-factor has been measured in the diffusive regime and is seen to increase with decreasing temperature. Earlier experiments were done in the ballistic regime, where the g-factor was found to be $g^* \approx 2.8$ and temperature independent[13].

Finally, we would like to note that the 2D electron system in silicon, used in this study, has a short-range disorder potential and constitutes a multi-valley system: features assumed in the theory. In other material systems, including GaAs/AlGaAs heterostructures and SiGe heterostructures, the disorder potential is long range, which leads to very high mobilities. The diffusive regime in these systems is therefore hard to reach at reasonable temperatures. In addition, high mobilities also imply very low carrier densities, which leads to a plethora of finite temperature corrections arising from non-degeneracy effects, large-r_s screening effects and so on. Therefore, the transition observed so far in these systems (see, for example, refs 14,15) might be a 'high'-temperature crossover phenomenon. Ultimately, however, at low enough temperatures the diffusive regime will unavoidably be reached. It remains to be seen whether or not the low-temperature behaviour in other 2D systems is quantitatively described by the two-parameter scaling theory.

References

1. Kravchenko, S. V. *et al.* Possible metal–insulator transition at $B = 0$ in 2 dimensions. *Phys. Rev. B* **50**, 8039–8042 (1994).
2. Abrahams, E., Anderson, P. W., Licciardello, D. C. & Ramakrishnan, T. V. Scaling theory of localization: Absence of quantum diffusion in two dimensions. *Phys. Rev. Lett.* **42**, 673–676 (1979).
3. Punnoose, A. & Finkel'stein, A. M. Metal–insulator transition in disordered two-dimensional electron systems. *Science* **310**, 289–291 (2005).
4. Punnoose, A. & Finkel'stein, A. M. Dilute electron gas near the metal–insulator transition: Role of valleys in silicon inversion layers. *Phys. Rev. Lett.* **88**, 016802 (2002).
5. Kravchenko, S. V. & Sarachik, M. P. Metal–insulator transition in two-dimensional electron systems. *Rep. Prog. Phys.* **67**, 1–44 (2004).
6. Shashkin, A. A. Metal–insulator transitions and the effects of electron–electron interactions in two-dimensional electron systems. *Phys.-Usp.* **48**, 129–149 (2005).
7. Finkel'stein, A. M. Influence of Coulomb interaction on the properties of disordered metals. *Sov. Phys.—JETP* **57**, 97–108 (1983).
8. Castellani, C., Di Castro, C., Lee, P. A. & Ma, M. Interaction-driven metal–insulator transitions in disordered fermion systems. *Phys. Rev. B* **30**, 527–543 (1984).
9. Finkel'stein, A. M. in *Electron Liquid in Disordered Conductors* (ed. Khalatnikov, I. M.) (Soviet Scientific Reviews, Vol. 14, Harwood Academic Publishers, London, 1990).
10. Lee, P. A. & Ramakrishnan, T. V. Magnetoresistance of weakly disordered electrons. *Phys. Rev. B* **26**, 4009–4012 (1982).
11. Castellani, C., Di Castro, C. & Lee, P. A. Metallic phase and metal–insulator transition in two-dimensional electronic systems. *Phys. Rev. B* **57**, 9381–9384 (1998).

12. Zala, G., Narozhny, B. N. & Aleiner, I. L. Interaction corrections at intermediate temperatures: Magnetoresistance in a parallel field. *Phys. Rev. B* **65**, 020201 (2002).

13. Anissimova, S. *et al.* Magnetization of a strongly interacting two-dimensional electron system in perpendicular magnetic fields. *Phys. Rev. Lett.* **96**, 046409 (2006).

14. Huang, J., Novikov, D. S., Tsui, D. C., Pfeiffer, L. N. & West, K. W. Non-activated transport of strongly interacting two-dimensional holes in GaAs. *Phys. Rev. B* **74**, 201302(R) (2006).

15. Lai, K. *et al.* Linear temperature dependence of conductivity in Si two-dimensional electrons near the apparent metal-to-insulator transition. *Phys. Rev. B* **75**, 033314 (2007).

Author contributions

The experiments were carried out by S.A. and S.V.K.; A.P. and A.M.F. were responsible for the theoretical analysis and T.M.K. provided the samples. All authors contributed to writing the manuscript.